ACS APPLIED MATERIALS & INTERFACES

Research Article

www.acsami.org

Mesoporous Zirconia Thin Films with Three-Dimensional Pore Structures and Their Application to Electrochemical Glucose Detection

Young-Seon Ko[†] and Young-Uk Kwon*[,†]

Department of Chemistry, BK-21 School of Chemical Materials Science, Sungkyunkwan University, Suwon 440-746, Korea

Supporting Information

ABSTRACT: Mesoporous zirconia thin films (MZFs) were synthesized using zirconium hydroxide sol particles and a structure directing agent, Pluronic F127 ($PEO_{106}PPO_{70}PEO_{106}$, EO = ethylene oxide, PO = propylene oxide). By controlling the F127/Zr ratio, we obtained two distinct MZFs with one in the *Fmmm* structure and the other in the $P6_3/mmc$ structure. The pore structures of these films were characterized by low-angle X-ray diffraction, grazing incidence small-angle X-ray scattering, electron microscopy, and N_2 sorption measurement. The *Fmmm* structure has interconnected pores and the $P6_3/mmc$ structure has less accessible pores. The MZFs were functionalized with glucose oxidase (GOx) and were studied for their potentials as an electrochemical sensor for glucose. The GOx-functionalized MZF electrodes show high sensitivity to glucose in a broad range of glucose concentration of 0.025 − 6.8 mM, which can be attributed to their biocompatibility providing a favorable microenvironment for GOx immobilization and to their 3D pore structures with good accessibility of pores.

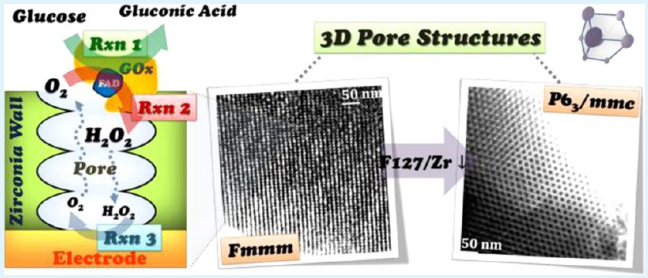

KEYWORDS: *mesoporous material, thin film, zirconia, 3D pore structure, glucose oxidase, electrochemical glucose sensor*

INTRODUCTION

Mesoporous materials are characterized by the controllable nanometer-sized pores.[1,2] By varying pore sizes, pore arrangements, and wall materials, various forms of mesoporous materials have emerged over the past two decades.[1−5] Most of the endeavors have been put in the mesoporous materials in powdery forms. Compared with the powdery forms, mesoporous materials in thin film forms are rather limited because of the several important restrictions in their syntheses.[6] As a result, the range of pore structures and wall materials in mesoporous thin films are much narrower than the powdery counterparts.

One of the motivations to study mesoporous thin films despite the difficult synthesis is the anticipation of their potential applications in various fields such as membranes, sensors, and nanoscopic functional materials.[7−11] In this regard, we considered that mesoporous thin films could be an ideal candidate for enzymatic biosensors because the large surface area and the ordered pore network could provide a favorable microenvironment for enzyme immobilization. Enzymatic biosensors have been used for the detection of ions and molecules in many biological, clinical, and environmental monitoring applications and gained considerable attention due to their simplicity and high sensitivity.[12] The immobilization of enzymes such as glucose oxidase (GOx) on metallic or metal oxide nanostructures has been achieved by methods such as self-assembly, physical adsorption, and incorporation in carbon paste, metal nanoparticles, and sol−gel oxides.[13−18] Compared with the typical nanoparticle electrodes, mesoporous thin film electrodes can have lower electric resistance and higher rates of mass transport for molecules to diffuse from the bulk solution to the electrode surface.[19,20]

Of the most studied materials of mesoporous thin films (silica, titania, and zirconia), zirconia appears to be the best suited for this purpose for its stability and biocompatibility.[21−23] Considering the nature of the surface to interact with enzymes, both titania and zirconia with about the same isoelectric points would work equally well. However, the absence of photocatalytic activity of zirconia can be an advantage over titania for stabilizing enzymes. In order to be used for this purpose, mesoporous zirconia thin films (MZFs) with accessible pores from the film surface and interconnected pores are required. While MZFs in the literature have a range of pore structures,[24−28] the majority of MZFs are reported to have the 2D-hexagonal pore structure,[26−28] which tends to align the pore channels parallel to the substrate and, thereby, the internal pores may not be readily accessible.[29] The requirement of pore accessibility can be satisfied with 3D pore structures.

In this study, we synthesized MZFs with two different pore morphologies by using presynthesized zirconium hydroxide sol

Received: December 26, 2012
Accepted: April 8, 2013
Published: April 8, 2013

solutions. This "nanoparticle route" approach has been successfully used for the synthesis of mesoporous titania thin films in the previous papers.[30] Those two types of MZFs have 3D pore structures with 9 nm-sized pores, desirable for the application to the enzymatic biosensor. We, therefore, immobilized GOx on these MZFs and demonstrated electrochemical detection of glucose with them.

EXPERIMENTAL SECTION

Synthesis of Zirconium Hydroxide Sols. To prepare a 0.9 M sol solution of zirconium hydroxide, 8.32 g of $ZrOCl_2 \cdot 8H_2O$ (Aldrich, 98%) was dissolved in 23.8 mL of anhydrous ethanol (Samchun, 99.9%) containing 1.00 mL of concentrated HCl (Samchun, 35.0 − 37.0%), which was followed by refluxing at 80 °C for at least 6 h.

Synthesis of Mesoporous Zirconia Thin Films. Coating solutions for the MZFs were prepared by dissolving Pluronic F127 ($PEO_{106}PPO_{70}PEO_{106}$, EO = ethylene oxide, PO = propylene oxide) in 4 g of the 0.9 M zirconium hydroxide sol synthesized, with subsequent stirring for 12 h. The F127/Zr molar ratio was varied between 0.003 and 0.007. The coating solutions were spin-coated on substrates, e.g., Si wafers or fluorine-doped tin oxide (FTO) glasses, at 8000 rpm for 40 s under a controlled relative humidity (RH) of 70−78% at 24−28 °C. The resulting films were then dried and aged at ca. 18 °C under a RH of ca. 85% for 24 h. The aged films were heated at 150 °C for 3−5 h and, then, calcined at 300 °C for 2 h to remove the surfactant. For the study of the thermal stability, the films were heated at 400, 450, or 500 °C for 10 min.

Fabrication of Glucose Oxidase-Functionalized Mesoporous Zirconia Thin Films. For the experiment on glucose detection, MZFs were first formed on FTO electrodes as described above, and, then, the resulting films were modified with GOx (EC 1.1.3.4 from *Aspergillus niger*, Sigma). The size of the FTO electrode was 1.5 × 0.7 cm^2 and the MZF covered an area of 1.2 × 0.7 cm^2 of it. The area modified with GOx was controlled to be fixed as ca. 0.4 cm^2. The immobilization of GOx was confirmed by Fourier transform infrared spectroscopy (Thermo Scientific Nicolet Avatar 320 spectrometer). To further improve the sensitivity to glucose, Pt was electrochemically deposited inside the pores of the MZF-modified FTO electrode (Pt@MZF). The electrodeposition condition was similar to that described in our previous paper[31] with a minor modification. A potential of −1.5 V was first applied for 0.1 s to form Pt nuclei uniformly, and a potential of −0.2 V was then imposed to grow them. A GOx solution was prepared by dissolving 20 mg of GOx in 4.0 mL of 0.1 M phosphate buffered saline (PBS, Sigma) solution at pH 7.1. To functionalize the films with GOx, 20 μL of the GOx solution was dropped onto the Pt@MZF or MZF electrode and was dried in ambient conditions. Subsequently, 10 μL of 0.1%-diluted Nafion (DuPont) as a binder to hold the GOx was spread onto the electrode surface and was dried at room temperature. For convenience, the GOx-modified electrodes will be denoted as GOx/Pt@MZF and GOx/MZF.

Structural Characterization of Mesoporous Zirconia Thin Films. The zirconium hydroxide sol solutions were characterized by dynamic light scattering (DLS, Malvern Zetasizer 1000HS) equipped with a 633 nm laser. The scattered light was detected at 90° to the incident beam. The sol solutions were dried at 40 °C overnight to obtain powder samples, which were analyzed by powder X-ray diffraction (XRD, Rigaku D/Max-2200, Cu Kα (λ = 1.5415 Å)) for the crystalline properties and energy dispersive X-ray spectroscopy (EDXS, Oxford Instruments INCA Penta FETx3) attached to a scanning electron microscope (SEM, JEOL JSM-7401F) for the elemental compositions.

The pore structures of the MZFs were characterized by low-angle XRD, SEM and transmission electron microscopy (TEM, JEOL JEM-3010). The crystalline properties of the wall materials were investigated by wide-angle XRD, high-resolution TEM (HRTEM), and selected area electron diffraction (SAED). For TEM and SAED, tiny slices of samples scrapped from the films were dispersed in ethanol and the resultant solution was then dropped on a carbon-coated Cu grid. To further acquire information on the pore structures, grazing incidence small-angle X-ray scattering (GISAXS) was conducted at the 4C2 Beamline of the Pohang Accelerator Laboratory (PAL).[32] A monochromatic X-ray radiation with the wavelength of 1.3807 Å was employed as the beam source and a two-dimensional charge-coupled device detector was used to collect the scattered signals. The sample-to-detector distance was 2165 mm, calibrated using polystyrene-*b*-polyethylene-*b*-polybutadiene-*b*-polystyrene block polymer. The incident X-ray angle was at 0.24−0.31°. The thickness of the MZFs was measured by cross-sectional SEM images.

N_2 adsorption−desorption isotherms at 77 K were obtained for powdery samples scrapped off the films on a Micromeritics TriStar II apparatus. Prior to the measurement, the samples were degassed at 160 °C under vacuum for 8 h. The specific surface area was calculated by Brunauer−Emmett−Teller (BET) method.[33] The pore volume and pore size distribution (PSD) were calculated using Barrett−Joyner−Halenda (BJH) method from the adsorption and the desorption branches of the isotherm.[34]

Electrochemical Characterization of Glucose Oxidase-Functionalized Mesoporous Zirconia Thin Films for Glucose Detection. All electrochemical measurements were carried out using a potentiostat (Ivium Compactstat) in a three-electrode system. A Ag/AgCl (saturated KCl) electrode and a Pt wire were employed as the reference electrode and the counter electrode, respectively. The GOx-modified electrodes prepared were used as the working electrodes whose geometric area was fixed as ca. 0.4 cm^2. A linear sweep voltammetry (LSV) was performed in air-saturated 0.1 M PBS solution with or without 10 mM β-D-(+)-glucose (Sigma) to investigate the possibility of the samples to glucose detection. Prior to the experiment, cyclic voltammetry (CV) was conducted in 0.1 M PBS solution, deoxygenated by N_2 gas for at least 15 min, at the sweep rate of 0.1 V s^{-1} for 20 min to clean the electrode surface. The quantitative evaluation for the glucose detection was carried out through chronoamperometry in which measured amounts of glucose were successively added into the air-saturated solution at intervals of 100 s under a controlled voltage of 0.6 V.

RESULTS AND DISCUSSION

In this study, we synthesized MZFs with two different pore morphologies and studied their potential application as a base material for the electrochemical glucose detection. We will first describe the synthesis and structural characterization of MZFs and then proceed to the description on the glucose detection.

Synthesis of Mesoporous Zirconia Thin Films. In general, the synthesis of mesoporous materials with transition metal oxides is much more limited compared with that of silica. It is mainly because of the fast reaction rates of the hydrolysis and condensation of transition metal ions causing phase segregation.[5] To overcome this problem, we first synthesized sol particles of zirconium hydroxide and employed a strongly acidic condition for the self-assembly process with a structure-directing agent (SDA) so that the zirconium hydroxide does not undergo any further hydrolysis and condensation reactions but just interacts with the SDA to form the desired self-assembly structures. In this regard, the zirconium hydroxide sol particles may be called as nanobuilding blocks (NBBs). Although there are a few cases in which mesoporous zirconia has been synthesized without the preparation of NBBs,[24−28] the NBB approach can be more reproducible and more versatile by allowing some degree of controls of the reaction conditions.[5]

Forced hydrolysis reactions of zirconium by refluxing $ZrOCl_2 \cdot 8H_2O$ in a strongly acidic ethanol solution produced zirconium hydroxide sol particles well suspended in the solution. The XRD patterns and EDXS data confirmed that the sol particles are zirconium hydroxide with stacked layered structure. (see Supporting Information for details.) The hydrodynamic diameter was determined to be 9 − 11 nm by

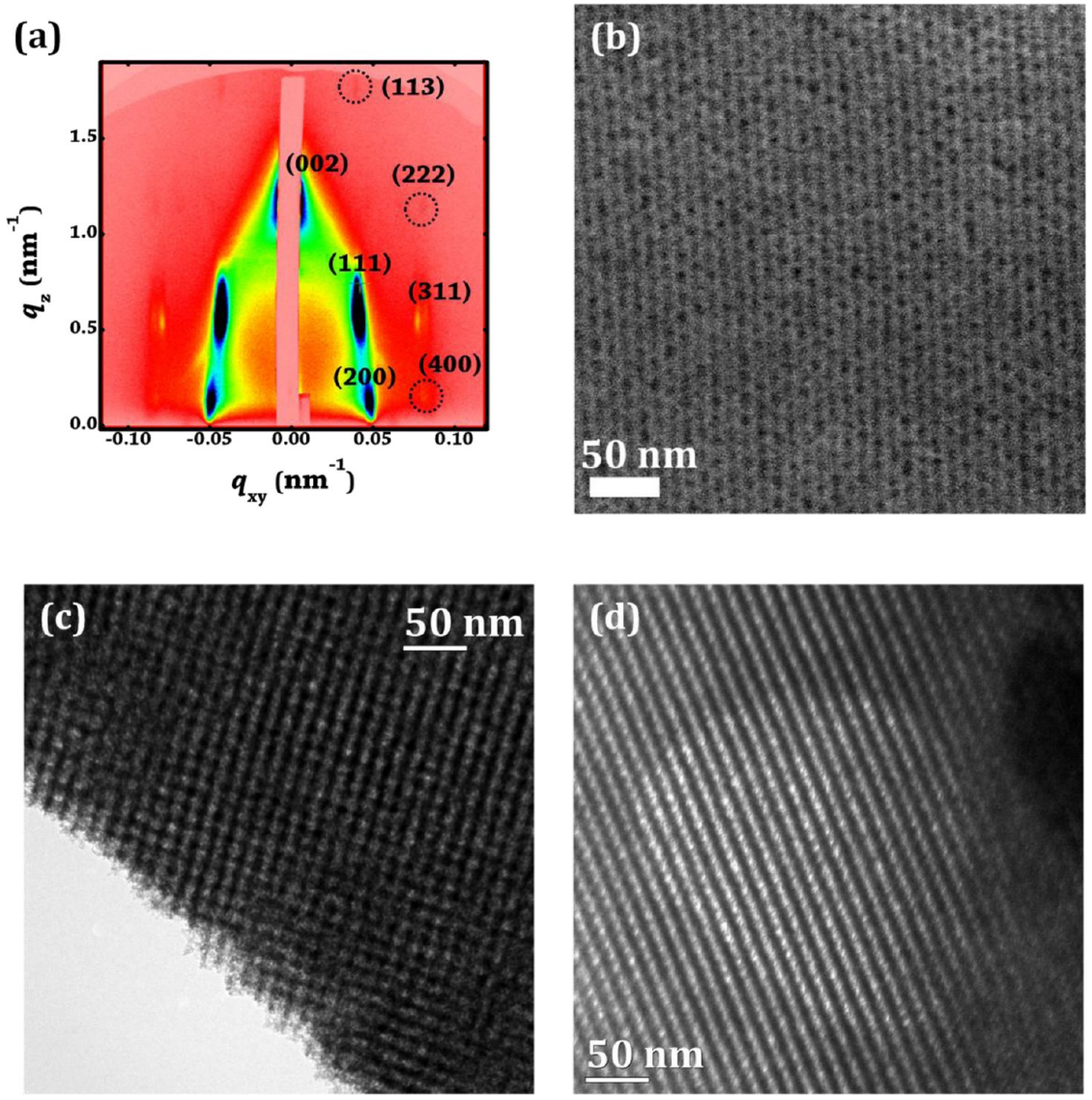

Figure 1. (a) 2D-GISAXS pattern and (b–d) electron microscopic images of MZF-1 showing *Fmmm* symmetry derived from a distorted $Im\bar{3}m$ symmetry: (b) SEM image of the film surface displaying the (002) plane; (c) TEM image of a (202) plane; (d) TEM image of a (002) plane. The samples of a, b, c, and d were calcined at 300, 300, 400, and 450 °C, respectively. The (002) and (202) planes in *Fmmm* structure correspond to (110) and (020) planes in $Im\bar{3}m$ structure, respectively.

DLS, suggesting nanoparticles considering the size of water layer on the particles (see Figure S1 in the Supporting Information).

By varying the F127/Zr molar ratio systematically, we found that two different pore structures were formed depending on the composition. We will denote the one from F127/Zr = 0.006 − 0.007 condition as MZF-1 and the other from F127/Zr = 0.003 − 0.005 MZF-2. The film thicknesses were measured to be 600 and 400 nm for MZF-1 and MZF-2, respectively, by cross-section SEM images (not shown here).

As will be seen below, the pore morphology of MZF-1 is a derivative of a body-centered cubic structure and that of MZF-2 a hexagonal close-packed structure. The occurrence of these 3D pore structures, as opposed to the 2D-hexagonal structures of MZFs in the literatures, is attributed to the NBB approach of the present study which leads to more curved hydrophilic/hydrophobic interfaces in the self-assembled mesophases. Apparently, the size of NBBs, the zirconium hydroxide sol particles, is larger than the zirconium oligomers or zirconium oxo clusters formed in the precursor solutions in the literature methods. Because the hydrophilic NBBs are readily combined with the PEO headgroups of the SDA, the volume of the headgroups is increased so that the curvature of hydrophilic/hydrophobic interface is changed.[4]

Structural Characterization of the Mesoporous Zirconia Thin Films. The 2D-GISAXS pattern of MZF-1 (Figure 1a) can be indexed with a face-centered orthorhombic (*Fmmm*) pore structure with cell parameters of a = 24 nm, b = 17 nm, and c = 10 nm. The SEM and TEM images in Figures 1b–d agree with this structural identification. This *Fmmm* structure has been observed in other mesoporous thin films. Its origin was explained as the formation of the cage-like $Im\bar{3}m$ structure oriented to have its [110] direction normal to the substrate and the contraction in this direction during the calcination step.[35,36] The lattice parameters (a_o, b_o, c_o) of the *Fmmm* unit cell before the contraction are related with that (a_c) of $Im\bar{3}m$ unit cell by $a_o = \sqrt{2}\, a_c$, $b_o = a_c$, $c_o = \sqrt{2}\, a_c$. From this relationship, we can calculate a_c as 17 nm. From the SEM

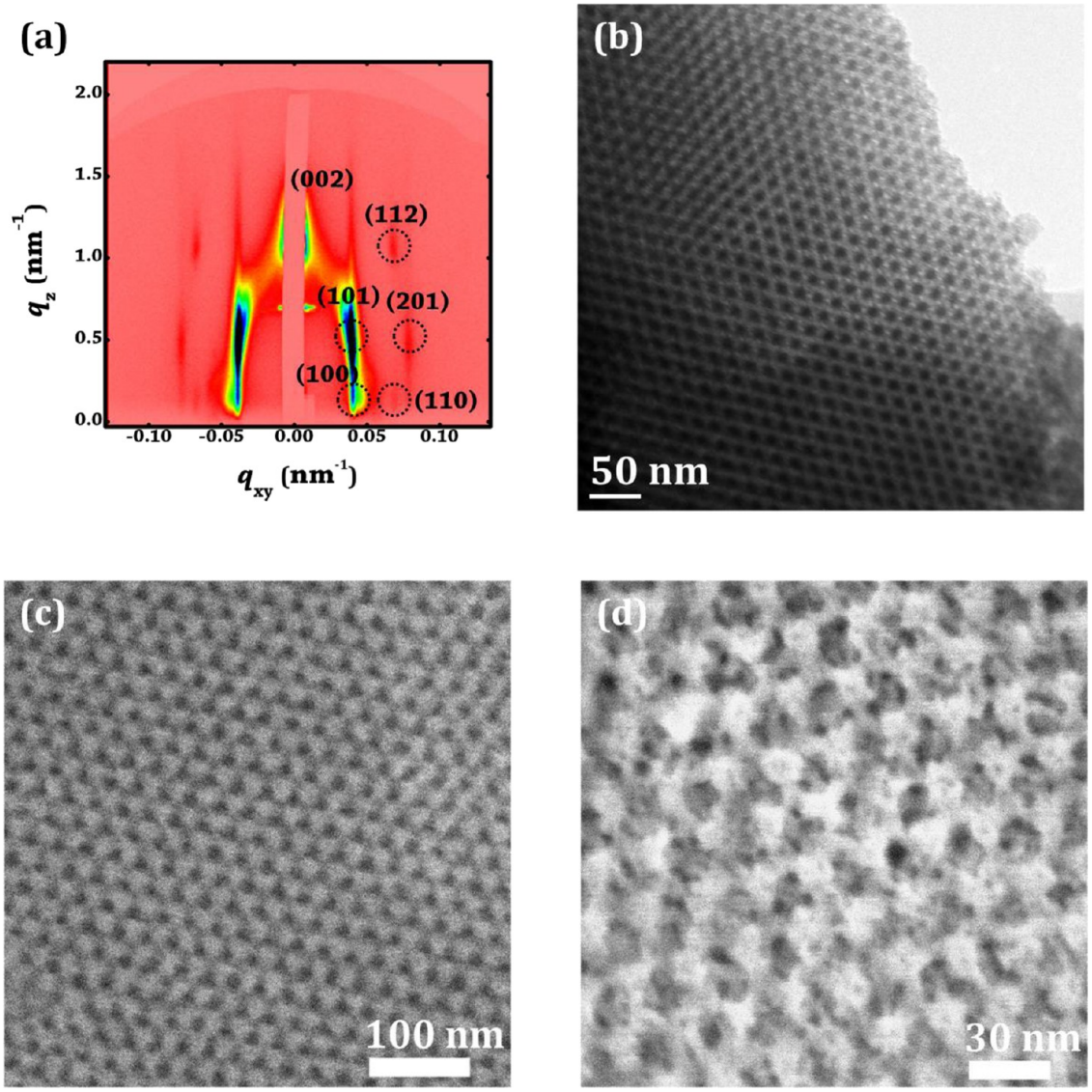

Figure 2. (a) 2D-GISAXS pattern of MZF-2 showing $P6_3/mmc$ symmetry, (b) TEM image, and (c, d) SEM images of the film surface representing (002) planes. The samples of a, b, c, and d were calcined at 300, 300, 400, and 500 °C, respectively.

images, the shortest pore-to-pore distance in the lateral dimension is measured to be 15 nm which agrees with the calculated value based on the lattice parameters and the orientation of the unit cell (= $\sqrt{(a_o^2 + b_o^2)}/2$); the pore size and the wall thickness are 9 and 6 nm, respectively. During the calcination, the uniaxial contraction along the c_o axis makes c_o be decreased by about 60% from 24 to 10 nm, whereas a_o and b_o remain unchanged. In fact, the degree of contraction depends on the calcination temperature and can be as large as about 70% when the temperature is raised to 500 °C (see Figures S2 and S3 in the Supporting Information).

The N_2 adsorption−desorption data on MZF-1 show a type IV isotherm with a H2 hysteresis loop (see Figure S4a in the Supporting Information), suggestive of a cagelike pore structure with the pores connected through pore openings.[1] BET surface area and pore volume were measured to be 197 $m^2\ g^{-1}$ and 0.18 $cm^3\ g^{-1}$, respectively. The surface area is comparable to but larger than those of mesoporous zirconia in the literatures, 97 − 163 $m^2\ g^{-1}$.[3,28,37,38] The PSD plot from the adsorption data (inset of Figure S4a in the Supporting Information) shows a broad peak encompassing the range smaller than 9 nm, indicating the presence of pores of various mean sizes probably because of the unidirectional contraction of the 9 nm sized pores and the smaller pore openings. By contrast, the PSD plot from the desorption data (inset of Figure S4a in the Supporting Information) shows a sharp peak at 3 nm, which appears to correspond to the small pore necks.

At lower F127/Zr molar ratios, a different structure emerged. The 2D-GISAXS pattern of MZF-2 (Figure 2a) shows three strong spots that can be indexed as (100), (101), and (002), and weak spots that can be indexed as (110), (201), and (112), characteristic of the $P6_3/mmc$ structure.[39] The unit cell is preferentially oriented to have its [001] direction normal to the substrate. The lattice parameters were measured to be $a = b =$ 18 nm and $c = 12$ nm. The TEM and SEM images (Figure 2b−d) agree with this structural identification. The shortest pore-to-pore distance in the lateral dimension is the same as the cell parameter of a, and both pore size and wall thickness are nearly equal to 9 nm. Compared with MZF-1, the thicker zirconia walls of MZF-2 can be explained as being due to the decreased F127/Zr ratio.

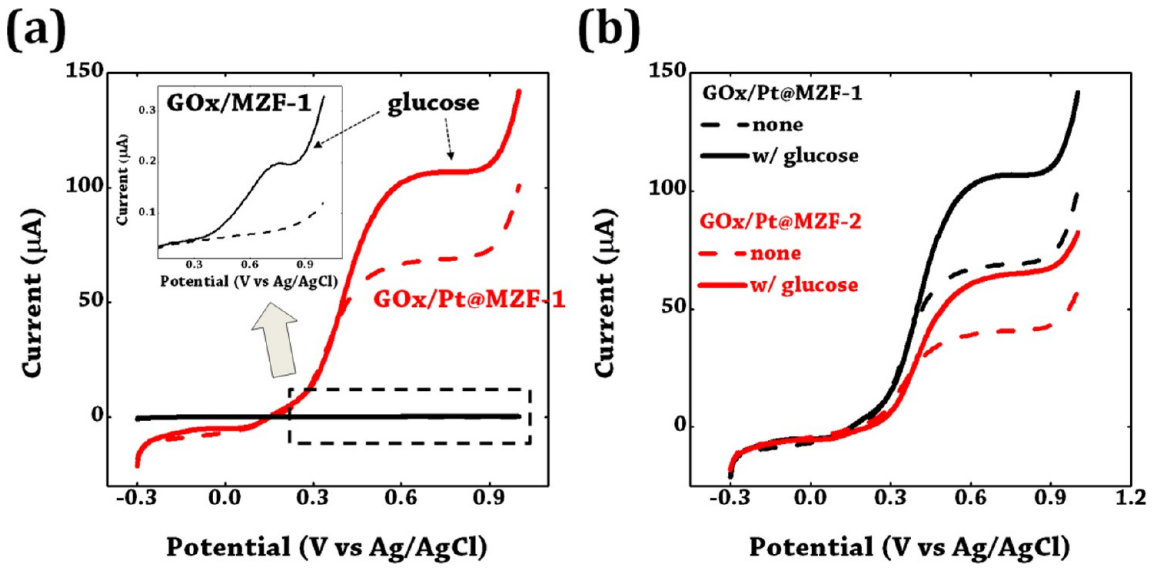

Figure 3. (a) Linear sweep voltammograms of GOx/MZF-1 (black lines) and GOx/Pt@MZF-1 (red lines) in a 0.1 M PBS solution without (dashed lines) and with 10 mM glucose (solid lines) at the scan rate of 20 mV s^{-1}. The inset depicts a magnified view of the current values of GOx/MZF-1. (b) Linear sweep voltammograms of GOx/Pt@MZF-1 (black lines) and GOx/Pt@MZF-2 (red lines) in a 0.1 M PBS solution without (dashed lines) and with 10 mM glucose (solid lines) at the scan rate of 20 mV s^{-1}.

This $P6_3/mmc$ structure is also known as the 3D-hexagonal structure whose ideal pore structure can be described as the hexagonal close (AB-type) packing of spherical cages.[39−41] Such AB stacking is clearly seen in the SEM and TEM images (Figure 2b−d). These images also show that the pore ordering of the film surface is remarkably well preserved up to 500 °C. By using low-angle XRD, we measured the degree of contraction along the [001] direction upon calcination, which turns out to be similar to that of MZF-1 (see Figure S2 in the Supporting Information).

The N_2 adsorption−desorption isotherm of MZF-2 is type IV with a H2 hysteresis loop, similar to that of MZF-1 (see Figure S4b in the Supporting Information). The BET surface area is 159 m^2 g^{-1} and the pore volume is 0.12 cm^3 g^{-1}. The PSD curve shows a broad peak in the range less than 5 nm. The smaller pore sizes of MZF-2 than MZF-1 appear to be related with the larger degree of contraction of MZF-2 than MZF-1 (see Figure S2c in the Supporting Information).

Based on the N_2 sorption results, the cages of the 3D hexagonal pore structure are also interconnected through necks. Generally, the $P6_3/mmc$ structure has limited pore accessibility with no or limited pore necks.[42] However, there are a few cases in which the pore interconnection is enhanced by calcination.[40,41] The N_2 sorption data of MZF-2 indicate that it belongs to this rarity. Probably because of the limited pore necks of the $P6_3/mmc$ structure, the pore accessibility of MZF-2 is expected to be smaller than that of MZF-1.

In the Pluronic copolymer−water systems, 2D-hexagonal ($p6m$) and 3D-cubic ($Ia\bar{3}d$ or $Im\bar{3}m$) pore structures have been frequently reported.[26,27,37,38] By contrast, the 3D-hexagonal pore structure ($P6_3/mmc$) as MZF-2 hardly forms in these systems. This is understood as arising from the nature of the Pluronic copolymer in which the contrast between the hydrophilic and hydrophobic parts is not so large. For the $P6_3/mmc$ structure to form, the interface of globular micelles is required to be more curved, which condition can be met with gemini surfactants having large effective head-groups[43] or nonionic surfactant with long chains.[1] In our case, the NBB approach makes the volume of the head-groups effectively large inducing the more curved interface. To the best of our knowledge, this is the first observation of the 3D-hexagonal pore structure for a MZF.

Immobilization of Glucose Oxidase and Electrochemical Glucose Detection. Zirconia has several beneficial properties for biological applications. Most of all, it is chemically inert and biocompatible. There are already several cases, in which zirconia has been used in biological and medical applications.[21−23,44,45] In addition to these attributes, for the case of electrochemical sensors, the 3D pore networks of zirconia materials can provide pore channels for transportation of ions and molecules to be detected. Therefore, our MZFs appear to be an ideal host of GOx as a redox enzyme to electrochemically detect glucose. The immobilization of GOx was achieved by dropping a GOx solution on MZFs calcined at 300 °C, followed by drying (see Figure S5 in the Supporting Information).

A frequently used method in GOx-based biosensors for glucose detection is to monitor H_2O_2, which is produced by the biocatalytic action of GOx as in the following reactions

$$\mathrm{GOx(FAD)} + \beta\text{-D-glucose} \rightarrow \mathrm{GOr(FADH_2)} + \delta\text{-D-gluconolactone} \quad (1)$$

$$\mathrm{GOr(FADH_2)} + \mathrm{O_2} \rightarrow \mathrm{GOx(FAD)} + \mathrm{H_2O_2} \quad (2)$$

$$\mathrm{H_2O_2} \rightarrow \mathrm{O_2} + 2\mathrm{H^+} + 2\mathrm{e^-} \quad (3)$$

where FAD is the oxidized form of the prosthetic group, flavin adenine dinucleotide.[44,45] Recently, Dionysios et al. reported that crystalline zirconia could function as the electron transfer medium at the electrode interface.[22] On the contrary, we found that the CV of GOx/MZF did not show any peak corresponding to the redox potential of $FAD/FADH_2$ which normally would appear at ca. −0.5 V (vs Ag/AgCl),[15] suggesting the absence of the direct electron transfer through the MZF. This may be because the zirconia wall in our MZF is amorphous. Therefore, the detection of glucose by our GOx/

dx.doi.org/10.1021/am303248p | ACS Appl. Mater. Interfaces 2013, 5, 3599−3606

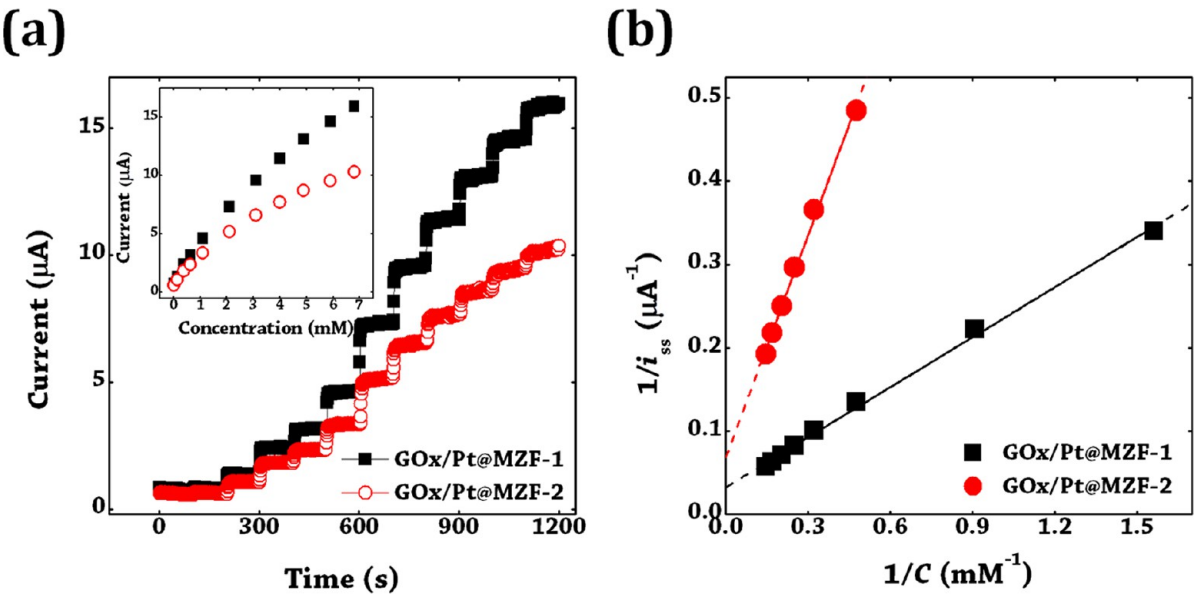

Figure 4. (a) Chronoamperometric responses of GOx/Pt@MZF-1 (black) and GOx/Pt@MZF-2 (red) with the stepwise addition of glucose into a 0.1 M PBS solution. The inset shows the corresponding calibration curves as a function of glucose concentrations. (b) Lineweaver–Burk-type plots for electrochemical determination of apparent Michaelis–Menten constants of GOx/Pt@MZF-1 (black) and GOx/Pt@MZF-2 (red). The straight lines are linear fits to the data points.

MZF electrode is through the transportation of O_2 and H_2O_2 to shuttle electrons.

In the LSV curves on the GOx/MZF-1 electrode with and without glucose, the H_2O_2 produced by eq 3 is detected as an anodic current at potentials higher than 0.3 V (vs Ag/AgCl) (inset of Figure 3a). However, the current is very small (<0.2 μA) probably because the FTO surface of GOx/MZF-1 has low activity for this reaction. In order to increase the sensitivity, we introduced Pt inside the pores of MZF (Pt@MZF) by electrochemical deposition. Pt is well-known as an excellent electrocatalyst for H_2O_2 oxidation.[46] The GOx/Pt@MZF-1 electrode prepared shows a 200 times increase of the anodic current from that of GOx/MZF-1. The similarly prepared GOx/Pt@MZF-2 also shows the activity to sense glucose (Figure 3b). The sensitivity of GOx/Pt@MZF-2 is slightly lower than GOx/Pt@MZF-1 probably due to the more constricted pore structure of MZF-2 than MZF-1. Without GOx, Pt@MZF electrode does not detect the presence of glucose (see Figure S6 in the Supporting Information), by which the possibility of direct glucose sensing is ruled out.

To quantitatively evaluate the performance of our samples for glucose detection, chronoamperometry studies were performed on GOx/Pt@MZF-1 and GOx/Pt@MZF-2 electrodes. The voltage was controlled to be 0.6 V (vs Ag/AgCl) at which H_2O_2 oxidation is diffusion-limited based on the LSV curves in Figure 3. The current–time transients in Figure 4a were acquired by successive addition of glucose from 0.025 to 6.8 mM into air-saturated 0.1 M PBS solutions. The response to the change in glucose concentration approaches the steady-state current within 10 s. The current–concentration plots in the inset of Figure 4a show that the current response is high at low glucose concentration and is slowly decreased with the glucose concentration. Similar concentration-dependent sensitivity behavior indicating saturation at higher concentrations has been observed in many other systems of electrochemical glucose detection.[15,16,44,45] Figure 4a shows that our glucose sensors have good response in the clinical concentration range. By approximating the plots as being composed of two linear segments, the sensitivities could be calculated. Three different electrodes were measured for each sample and the results are shown in Table 1. After storing the electrodes for 135 days at 4 °C in air, GOx/Pt@MZF-1 showed a reduction of signal intensity by 61% and GOx/Pt@MZF-2 by 70% from those of freshly prepared electrodes.

Table 1. Sensitivities of GOx/Pt@MZF Electrodes

sample	sensitivity (μA mM^{-1})[a]	
concentration range of glucose	0.025–1.1 mM	2.1–6.8 mM
GOx/Pt@MZF-1	3.26 ± 0.80	1.80 ± 0.35
GOx/Pt@MZF-2	1.92 ± 0.89	1.04 ± 0.35

[a]Calculated by the linear fit to current-concentration data of three different electrodes and averaged.

There are numerous reports on the electrochemical glucose detection.[12–18,44–47] Unfortunately, the performance data in those reports are presented in widely different ways, making direct comparison with our data almost impossible. Nevertheless, it seems reasonable to say that the sensitivity of a glassy carbon electrode modified by Pt nanoparticles and, then, by GOx represents a medium value, 4.1 μA mM^{-1}.[46] Compared with this, our GOx/Pt@MZF electrodes show lower sensitivity. However, zirconia has the advantage of higher biocompatibility than carbon-based materials, which may offset the slightly smaller sensitivity.

On the other hand, the sensitivity data of our GOx/Pt@MZF electrodes compare well with those of Zr-based electrodes such as a sol–gel ZrO_2/chitosan composite (0.028 μA mM^{-1})[44] and zirconium hydrogenphosphate (0.14 nA mM^{-1})[47] as GOx immobilization matrices. Probably, the 3D pore structures of the MZFs allow molecules such as glucose, O_2, and H_2O_2, to be freely transported through the pores. At the same time, the pores of MZFs are more confined compared with the pores of other sensors. Therefore, reporter H_2O_2 molecules have smaller

chances to escape the pores in our GOx/Pt@MZF electrodes making the detection efficiency higher than in the literature cases. Kim et al. reported a sensitivity of 3.40 μA mM^{-1} on a sol−gel zirconia/Nafion composite.[45] However, it appears that the GOx loading in their work was at least three times higher than ours.

Between the two GOx/Pt@MZF electrodes, GOx/Pt@MZF-1 shows about 50% higher sensitivity than GOx/Pt@MZF-2. The reason appears to be related with the higher pore accessibility of MZF-1 than MZF-2. The effect of pore accessibility can be also seen in the kinetics data on the enzyme reaction. The apparent Michaelis−Menten constant, K_M^{app}, for immobilized GOx can be determined electrochemically by using the modified Lineweaver−Burk equation

$$\frac{1}{i_{ss}} = \left(\frac{K_M^{app}}{i_{max}}\right)\left(\frac{1}{C}\right) + \frac{1}{i_{max}} \quad (4)$$

where i_{ss} and i_{max} are the steady-state current after the glucose addition and the maximum current under the saturation condition of glucose, respectively, and C is the concentration of glucose. The lower K_M^{app} value means the better biocatalytic action of GOx. From the plots of i_{ss} vs $1/C$ (Figure 4b), K_M^{app} values of GOx/Pt@MZF-1 and GOx/Pt@MZF-2 were calculated to be 6.1 and 11.6 mM, respectively. The K_M^{app} value is affected by two factors, the reaction kinetics of GOx and the mass transport of reporter molecules to the electrode. Generally, the effects of the two factors cannot be separated in the electrochemical method.[48] In the present case, however, assuming that the pore structures do not influence the intrinsic catalytic property of immobilized GOx, the difference of K_M^{app} between the two GOx/Pt@MZF electrodes can be attributed to the different transport properties of O_2 and H_2O_2 through the pores of MZFs. That is, MZF-1 with the higher porosity shows a higher rate of mass transport than MZF-2 with the lower porosity. In fact, the K_M^{app} of GOx/Pt@MZF-1 electrode is close to the intrinsic Michaelis−Menten constant (K_M) of GOx in the bulk solution, 6.8 mM, obtained by spectroscopic methods in ref 48, indicating that the mass transport in MZF-1 is very fast.

CONCLUSIONS

In this study, we synthesized MZFs with two different pore morphologies with one an orthorhombic derivative of the $Im\bar{3}m$ structure and the other a hexagonal close-packed structure. Both the films have 3D interconnected pore networks with very uniform pore diameters of 9 nm; the former has interconnected pore network exhibiting good pore accessibility and the pores of the latter are less accessible from the film surface. The MZFs were fabricated into electrochemical biosensors for glucose detection through modification with Pt deposition and GOx immobilization. The electrochemical data of GOx/Pt@MZF-1 electrode show that it has higher sensitivity than the Zr-based glucose sensors in the literatures, which can be attributed to the favorable surface chemistry of zirconia and the 3D pore structure of the MZF. The simple method to fabricate a biosensor can also be exploited to immobilize other enzymes and bioactive molecules on various 3D metal oxide nanostructures to form versatile electrodes for biosensor studies.

ASSOCIATED CONTENT

Supporting Information

DLS, XRD, and EDXS data for the characterization of zirconium hydroxide sols, low-angle and wide-angle XRD patterns of MZFs with heating temperature, HRTEM and SAED data for the crystallization of MZFs, N_2 adsorption−desorption isotherms and the corresponding PSD plots of MZFs, FT-IR spectra confirming the GOx immobilization, and LSV curves of Pt@MZF for glucose detection. This material is available free of charge via the Internet at http://pubs.acs.org.

AUTHOR INFORMATION

Corresponding Author

*E-mail: ywkwon@skku.edu.

Author Contributions

†The manuscript was written through equal contributions of both authors. All authors have given approval to the final version of the manuscript.

Notes

The authors declare no competing financial interest.

ACKNOWLEDGMENTS

This work was supported by Grants NRF-20090081018 (Basic Science Research Program), NRF-2010-0029698 (Priority Research Center Program), NRF-2011-0006268 (Basic Science Research Program), and the Agency for Defense Development through Chemical and Biological Defense Research Center. We thank CCRF for TEM data and PAL for synchrotron GISAXS data. We also thank Dr. M. Shahid for helpful discussion on electrochemical glucose detection and Prof. J. M. Kim, Dr. J. H. Kim, and Mr. S.-B. Park for useful discussion on N_2 sorption measurement.

REFERENCES

(1) Zhao, D.; Huo, Q.; Feng, J.; Chmelka, B. F.; Stucky, G. D. *J. Am. Chem. Soc.* **1998**, *120*, 6024−6036.
(2) Sakamoto, Y.; Kaneda, M.; Terasaki, O.; Zhao, D.; Kim, J. M.; Stucky, G. D.; Shin, H. J.; Ryoo, R. *Nature* **2000**, *408*, 449−453.
(3) Yang, P.; Zhao, D.; Margolese, D. I.; Chmelka, B. F.; Stucky, G. D. *Chem. Mater.* **1999**, *11*, 2813−2826.
(4) Kim, J. M.; Sakamoto, Y.; Hwang, Y. K.; Kwon, Y.-U.; Terasaki, O.; Park, S.-E.; Stucky, G. D. *J. Phys. Chem. B* **2002**, *106*, 2552−2558.
(5) Sanchez, C.; Boissière, C.; Grosso, D.; Laberty, C.; Nicole, L. *Chem. Mater.* **2008**, *20*, 682−737.
(6) Grosso, D.; Cagnol, F.; Soler-Illia, G. J. A. A.; Crepaldi, E. L.; Amenitsch, H.; Brunet-Bruneau, A.; Bourgeois, A.; Sanchez, C. *Adv. Funct. Mater.* **2004**, *14*, 309−322.
(7) Lu, Y.; Ganguli, R.; Drewien, C. A.; Anderson, M. T.; Brinker, C. J.; Gong, W.; Guo, Y.; Soyez, H.; Dunn, B.; Huang, M. H.; Zink, J. I. *Nature* **1997**, *389*, 364−368.
(8) Otal, E. H.; Angelomé, P. C.; Bilmes, S. A.; Soler-Illia, G. J. A. A. *Adv. Mater.* **2006**, *18*, 934−938.
(9) Renault, C.; Balland, V.; Martinez-Ferrero, E.; Nicole, L.; Sanchez, C.; Limoges, B. *Chem. Commun.* **2009**, 7494−7496.
(10) Qi, H.; Shopsowitz, K. E.; Hamad, W. Y.; MacLachlan, M. J. *J. Am. Chem. Soc.* **2011**, *133*, 3728−3731.
(11) Kim, Y.-T.; Han, J. H.; Hong, B. H.; Kwon, Y.-U. *Adv. Mater.* **2010**, *22*, 515−518.
(12) Wang, J. *Chem. Rev.* **2008**, *108*, 814−825.
(13) Xiao, Y.; Patolsky, F.; Katz, E.; Hainfeld, J. F.; Willner, I. *Science* **2003**, *299*, 1877−1881.
(14) Cai, C.; Chen, J. *Anal. Biochem.* **2004**, *332*, 75−83.
(15) Zhao, S.; Zhang, K.; Bai, Y.; Yang, W.; Sun, C. *Bioelectrochemistry* **2006**, *69*, 158−163.

(16) Wei, A.; Sun, X. W.; Wang, J. X.; Lei, Y.; Cai, X. P.; Li, C. M.; Dong, Z. L.; Huang, W. *Appl. Phys. Lett.* **2006**, *89*, 123902−123904.
(17) Shan, C.; Yang, H.; Song, J.; Han, D.; Ivaska, A.; Niu, L. *Anal. Chem.* **2009**, *81*, 2378−2382.
(18) Dai, Z.; Shao, G.; Hong, J.; Bao, J.; Shen, J. *Biosens. Bioelectron.* **2009**, *24*, 1286−1291.
(19) Etienne, M.; Grosso, D.; Boissière, C.; Sanchez, C.; Walcarius, A. *Chem. Commun.* **2005**, 4566−4568.
(20) Fattakhova-Rohlfing, D.; Brezesinski, T.; Rathouský, J.; Feldhoff, A.; Oekermann, T.; Wark, M.; Smarsly, B. *Adv. Mater.* **2006**, *18*, 2980−2983.
(21) Liang, R.; Deng, M.; Cui, S.; Chen, H.; Qiu, J. *Mater. Res. Bull.* **2010**, *45*, 1855−1860.
(22) Chen, Y.; Lunsford, S. K.; Song, Y.; Ju, H.; Falaras, P.; Likodimos, V.; Kontos, A. G.; Dionysiou, D. D. *Chem. Eng. J.* **2011**, *170*, 518−524.
(23) Liu, B.; Hu, J.; Foord, J. S. *Electrochem. Commun.* **2012**, *19*, 46−49.
(24) Wang, K.; Morris, M. A.; Holmes, J. D.; Yu, J.; Xu, R. *Microporous Mesoporous Mater.* **2009**, *117*, 161−164.
(25) Mikó, A.; Demirel, A. L.; Somer, M. *J. Mater. Chem.* **2012**, *22*, 3705−3707.
(26) Crepaldi, E. L.; Soler-Illia, G. J. A. A.; Grosso, D.; Sanchez, C. *New J. Chem.* **2003**, *27*, 9−13.
(27) Soler-Illia, G. J. A. A.; Crepaldi, E. L.; Grosso, D.; Sanchez, C. *J. Mater. Chem.* **2004**, *14*, 1879−1886.
(28) Fang, H.; Wan, T.; Shi, W.; Zhang, M. *J. Non-Cryst. Solids* **2007**, *353*, 1657−1661.
(29) Lee, U.-H.; Kim, M.-H.; Kwon, Y.-U. *Bull. Korean Chem. Soc.* **2006**, *27*, 808−816.
(30) Lee, U.-H.; Lee, H.; Wen, S.; Mho, S.-I.; Kwon, Y.-U. *Microporous Mesoporous Mater.* **2006**, *88*, 48−55.
(31) Ko, Y.-S.; Kwon, Y.-U. *Electrochim. Acta* **2010**, *55*, 7276−7281.
(32) Lee, B.; Park, I.; Yoon, J.; Park, S.; Kim, J.; Kim, K.-W.; Chang, T.; Ree, M. *Macromolecules* **2005**, *38*, 4311−4323.
(33) Gregg, S. J.; Sing, K. S. W. *Adsorption, Surface Area and Porosity*, 2nd ed.; Academic Press: London, 1982; pp 168−169.
(34) Barrett, E. P.; Joyner, L. G.; Halenda, P. P. *J. Am. Chem. Soc.* **1951**, *73*, 373−380.
(35) Falcaro, P.; Grosso, D.; Amenitsch, H.; Innocenzi, P. *J. Phys. Chem. B* **2004**, *108*, 10942−10948.
(36) Urade, V. N.; Hillhouse, H. W. *J. Phys. Chem. B* **2005**, *109*, 10538−10541.
(37) Tian, B.; Yang, H.; Liu, X.; Xie, S.; Yu, C.; Fan, J.; Tu, B.; Zhao, D. *Chem. Commun.* **2002**, 1824−1825.
(38) Yuan, Q.; Li, L.-L.; Lu, S.-L.; Duan, H.-H.; Li, Z.-X.; Zhu, Y.-X.; Yan, C.-H. *J. Phys. Chem. C* **2009**, *113*, 4117−4124.
(39) Grosso, D.; Balkenende, A. R.; Albouy, P. A.; Lavergne, M.; Mazerolles, L.; Babonneau, F. *J. Mater. Chem.* **2000**, *10*, 2085−2089.
(40) Wu, C.-W.; Ohsuna, T.; Kuwabara, M.; Kuroda, K. *J. Am. Chem. Soc.* **2006**, *128*, 4544−4545.
(41) Jiang, X.; Oveisi, H.; Nemoto, Y.; Suzuki, N.; Wu, K. C.-W.; Yamauchi, Y. *Dalton Trans.* **2011**, *40*, 10851−10856.
(42) Sakamoto, Y.; Díaz, I.; Terasaki, O.; Zhao, D.; Pérez-Pariente, J.; Kim, J. M.; Stucky, G. D. *J. Phys. Chem. B* **2002**, *106*, 3118−3123.
(43) Huo, Q.; Leon, R.; Petroff, P. M.; Stucky, G. D. *Science* **1995**, *268*, 1324−1327.
(44) Yang, Y.; Yang, H.; Yang, M.; Liu, Y.; Shen, G.; Yu, R. *Anal. Chim. Acta* **2004**, *525*, 213−220.
(45) Kim, H.-J.; Yoon, S. H.; Choi, H. N.; Lyu, Y.-K.; Lee, W.-Y. *Bull. Korean Chem. Soc.* **2006**, *27*, 65−70.
(46) Luhana, C.; Bo, X.-J.; Ju, J.; Guo, L.-P. *J. Nanopart. Res.* **2012**, *14*, 1158−1166.
(47) Park, S.; Chung, T. D.; Kang, S. K.; Jeong, R.-A; Boo, H.; Kim, H. C. *Anal. Sci.* **2004**, *20*, 1635−1638.
(48) Kamin, R. A.; Wilson, G. S. *Anal. Chem.* **1980**, *52*, 1198−1205.